

Charge Transfer in the P(g₄2T-T):BBL Organic Polymer Heterojunction Measured with Core-Hole Clock Spectroscopy

Elin Berggren,* Yi-Chen Weng, Qifan Li, Chi-Yuan Yang, Fredrik O. L. Johansson, Ute B. Cappel, Magnus Berggren, Simone Fabiano, and Andreas Lindblad



Cite This: *J. Phys. Chem. C* 2023, 127, 23733–23742



Read Online

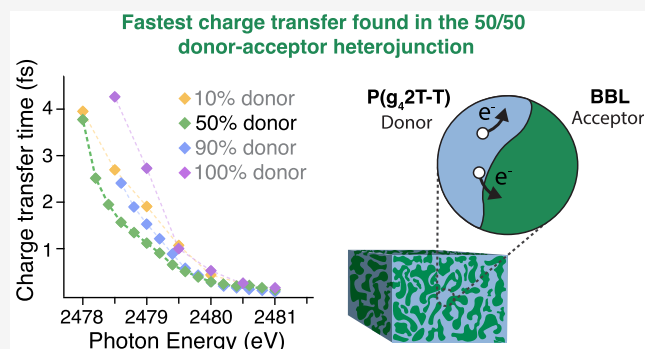
ACCESS |

Metrics & More

Article Recommendations

Supporting Information

ABSTRACT: The conductivity of organic polymer heterojunction devices relies on the electron dynamics occurring along interfaces between the acceptor and donor moieties. To investigate these dynamics with chemical specificity, spectroscopic techniques are employed to obtain localized snapshots of the electron behavior at selected interfaces. In this study, charge transfer in blends (by weight 10, 50, 90, and 100%) of p-type polymer P(g₄2T-T) (bithiophene-thiophene) and n-type polymer BBL (poly(benzimidazo-benzo-phenanthroline)) was measured by resonant Auger spectroscopy. Electron spectra emanating from the decay of core-excited states created upon X-ray absorption in the donor polymer P(g₄2T-T) were measured in the sulfur *KL*_{2,3}*L*_{2,3} Auger kinetic energy region as a function of the excitation energy. By tuning the photon energy across the sulfur K-absorption edge, it is possible to differentiate between decay paths in which the core-excited electron remained on the atom with the core-hole and those where it tunneled away. Analyzing the competing decay modes of these localized and delocalized (charge-transfer) processes facilitated the computation of charge-transfer times as a function of excitation energy using the core-hole clock method. The electron delocalization times derived from the measurements were found to be in the as/fs regime for all polymer blends, with the fastest charge transfer occurring in the sample with an equal amount of donor and acceptor polymer. These findings highlight the significance of core-hole clock spectroscopy as a chemically specific tool for examining the local charge tunneling propensity, which is fundamental to understanding macroscopic conductivity. Additionally, the X-ray absorption spectra near the sulfur K-edge in the P(g₄2T-T) polymer for different polymer blends were analyzed to compare molecular structure, orientation, and ordering in the polymer heterojunctions. The 50% donor sample exhibited the most pronounced angular dependence of absorption, indicating a higher level of ordering compared to the other weight blends. Our studies on the electron dynamics of this type of all-polymer donor–acceptor systems, in which spontaneous ground-state electron transfer occurs, provide us with critical insights to further advance the next generation of organic conductors with mixed electron–hole conduction characteristics suitable for highly stable electrodes of relevance for electronic, electrochemical, and optoelectronic applications.



INTRODUCTION

Organic polymer heterojunctions have gained significant attention in the field of electronic and optoelectronic devices due to their unique properties and potential for cost-effective fabrication. Their low cost, versatile chemical synthesis, and chemical functionality, combined with high electrical conductivity in both p-type (hole-transporting) and n-type (electron-transporting) polymers make polymer heterojunctions specifically interesting and excellent candidates for an array of applications.¹

Thiophene-based conjugated polymer systems have extensively been studied for applications in organic photovoltaics, organic field-effect transistors, and neuronal interconnects.² Bulk heterojunctions can be created by combining p- and n-type semiconductors. These heterojunctions can facilitate

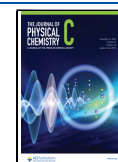
charge transfer through excitations such as photon absorption. As a result, excitons can be separated, and the electrons and holes can be transported to the harvesting electrodes. Such organic bulk heterojunctions have extensively been used in solar cells due to their cost-effectiveness and recyclability, which is especially important in meeting the increasing demands for energy consumption.^{3–5}

Received: August 22, 2023

Revised: November 20, 2023

Accepted: November 20, 2023

Published: December 5, 2023



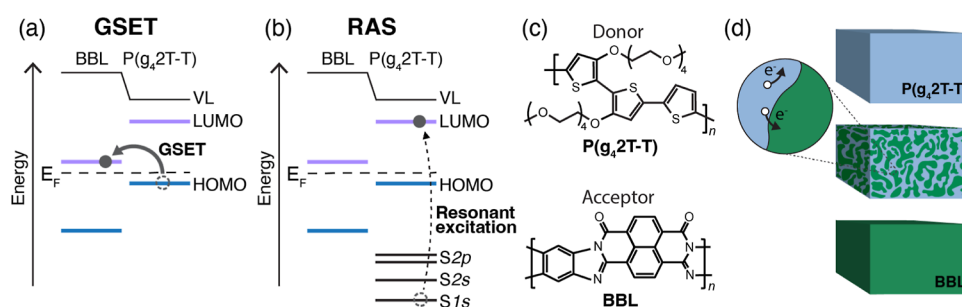


Figure 1. (a) Energy diagrams of the P(g₄,2T-T):BBL polymer heterojunction showing the spontaneous GSET and (b) resonant excitation (dotted arrow) from the S 1s energy level in RAS measurements. (c) Molecular structures of the donor and acceptor polymer. (d) Schematic view of polymer heterojunctions with illustration of intra- and intermolecular charge transfer following X-ray excitation.

Recently, polymer heterojunctions, based on p- and n-type conjugated polymers with large vacuum level offset, have resulted in spontaneous electron transfer from the ground state.⁶ Those all-polymer conductor systems define self-organized bicontinuous mixed electron–hole conductor systems with a promising use as the conductor, electrode, or electroactive layer in various electronic, electrochemical, and bioelectronic applications. As the p- and n-type conjugated polymers are mutually charge-compensating each other in those systems, via ground-state electron transfer (GSET), mixed electron–hole conduction is achieved without any addition of nonconducting dopants, such as the addition of polyelectrolytes or doping ions. The resulting all-polymer material system therefore provides high combined electron and hole conductivity being stable at elevated temperatures and while exposed to an array of harsh chemical conditions. In order to optimize such all-polymer mixed electron–hole conductors, with respect to, for example, improved and balanced electron and hole conductivity and temperature stability, in-depth knowledge of the dynamics of electron-transfer characteristics is needed of such polymer blends. When the n-type polymer poly-(benzimidazobenzophenanthroline) (BBL) is paired with the p-type polymer bithiophene-thiophene [P(g₄,2T-T)], being a low-ionization energy donor polymer, a large shift in the vacuum level is reached (0.55 eV) at the interface. See Figure 1c for the molecular structures. This allows for spontaneous GSET (Figure 1a) to take place at the interface of the molecular heterojunction (Figure 1d). In the studied system, GSET occurs at an efficiency of 2%.⁶

Xu and co-workers⁶ used ultraviolet photoelectron spectroscopy and inverse photoelectron spectroscopy to infer the energy level alignment for the P(g₄,2T-T):BBL system in Figure 1a,b and relate those results to macroscopic conductivity measurements. The macroscopic conductivity depends on charge transfer along and between polymer chains, which in these kinds of systems also depend on the relative amount of constituents and the ordering between them.

In this study, we want to investigate how tunneling propensity from electrons in excited states (which manifest orbital overlap which in turn depend on energy alignment and the orientation between molecules) change as a function of the relative concentration between the two different polymers and if this can be related to macroscopic conductivity of the system.

By exciting a core-electron (e.g., from the S 1s) with X-rays, a core-excited state can be prepared with a hole in the core-orbital and an electron in a previously unoccupied orbital. If

the total cross section of this process is studied as a function of X-ray energy, we obtain information about the unoccupied states in the system and the orientation of the molecules (XAS/NEXAFS).⁷ The core-excited state is metastable and will decay in some manner with an electron filling the core-hole; the excess energy may be carried away with an X-ray photon or in a radiationless decay wherein an electron is emitted. The latter process is called a resonant Auger decay and can be studied by resonant Auger spectroscopy (RAS).⁸

If the excited electron is involved in the decay directly, we have a coherent process which is local in the sense that the surrounding only slightly perturbs the process and only decay channels related to orbitals on the site of excitation are involved in the process. This “localized” decay leads to a singly charged final state. Here, we consider the spectator decay channel, where the core-excited electron remains on the site of the excitation during the decay of the core-hole. We also refer to this as the localized Raman decay. (A participator, where the core-excited electron fills the core-hole, can also occur but the kinetic energy of the electrons emanating from that decay is much higher than those considered here.) There are decay channels that involve the core-excited electron tunneling away from the site of excitation, thus becoming decoupled from the site of the core-hole (incoherent channel), which can then decay by a process resembling a normal Auger decay leading to a doubly charged final state. By comparing the propensity for the local and nonlocal processes measured as a function of X-ray energy, one can infer the occurrence of core-excited electrons tunneling away from the site of excitation. From this, we can determine charge-transfer rates in this prepared state using the lifetime of the core-hole as an internal time reference.⁹ This is the basis for core-hole clock (CHC) spectroscopy which can be used to measure orbital overlap strengths and variations of the density of states available for tunneling^{10–12} with chemical¹³ and even orbital specificity^{14–16} if polarized, tunable X-rays are used on well-defined samples.

To exemplify, in this study, sulfur 1s electrons are excited to the lowest unoccupied molecular orbital (LUMO), or other unoccupied orbitals, depicted by the dotted line in Figure 1b, and the delocalization time (charge-transfer time) of this electron is determined in the manner outlined above.

Below, we explore in detail electronic structure, molecular orientation, and charge dynamics in polymer bulk heterojunction blends composed of acceptor polymer BBL and donor polymer P(g₄,2T-T) with weight percentages of P(g₄,2T-T) in relation to BBL at 10, 50, 90, and 100%. The combination of X-ray based techniques allows us to discuss the efficiency of

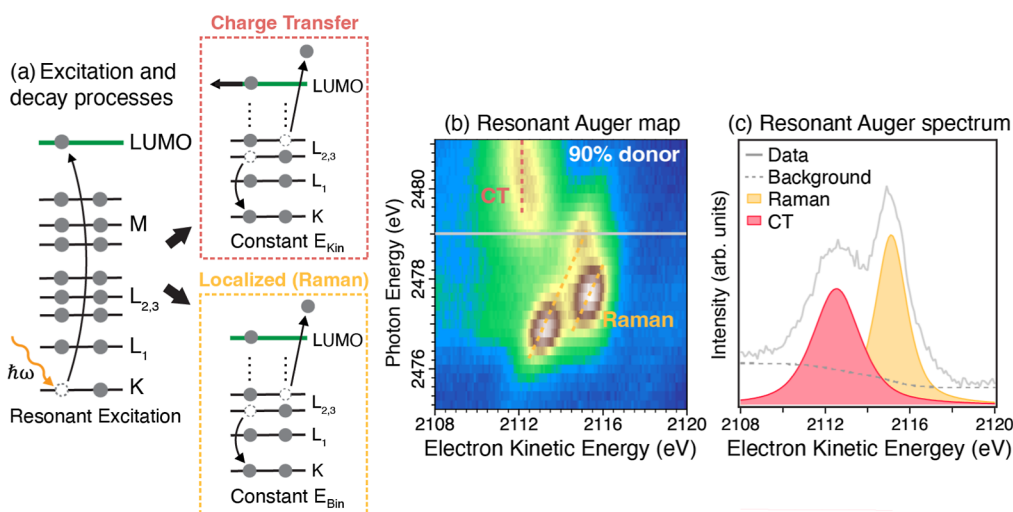


Figure 2. (a) Schematic view of resonant K-shell excitation followed by either a localized Raman decay (yellow) or delocalized charge transfer (CT) followed by Auger-like decay (red). (b) Resonant Auger 2D map of the sulfur K-edge region in the 90% donor sample with CT and Raman channel marked with red and yellow dotted lines. (c) Spectral fit of the Auger spectrum at a photon energy of 2479 eV (gray horizontal line in the Auger map).

charge transfer in these polymer blends from an orbital and molecular ordering perspective.

METHODS

Sample Preparation. Heterojunction samples of polymers BBL and P(g₄2T-T) were prepared by spin-coating the blends soluted in methanesulfonic acid (MSA) on to Cr/Au on Si substrates at 2000 rpm for 1 min. More information about sample preparation can be found elsewhere.¹⁷ The samples were thereafter annealed at 120 °C in an argon atmosphere for 30 min. The weight percentage of the donor polymer P(g₄2T-T) with respect to the acceptor BBL were 10, 50, 90, and 100%. Samples were kept in an argon atmosphere prior to spectroscopic measurements. The polymer film thickness was measured to 150 nm by using a stylus profiler (DektakXT).

X-ray-Based Electron Spectroscopies. All spectroscopic measurements were conducted at the HIKE endstation located at the KMC-1 beamline at the synchrotron facility BESSY II. Equipped with a double crystal monochromator, this endstation reaches a photon flux of 10¹² photons/s in a beam spot of 0.3 × 0.4 mm. The beamline resolution is 0.3 eV at the excitation energy used in this work.¹⁸ Measurements were performed using a Scienta R4000 hemispherical electron energy analyzer with a 200 eV pass energy for Auger electrons and photoelectrons. Experimental energy resolution was obtained by fitting Au 4f core level spectra using a lifetime broadening of 0.3 and 0.28 eV for the 7/2 and 5/2 spin–orbit components.¹⁹ For sample characterization, the obtained resolution is 0.48 eV (photon energy 3000 eV) and for resonant Auger measurements the resolution is 0.45 eV (excitation energies 2460–2500 eV). The samples were positioned with a 78° angle between the sample surface and the axis of the hemispherical analyzer and 12° to the incoming light. Spectroscopic data were analyzed in Igor Pro (7.08), using the SPANCF fitting procedures.²⁰ Auger and Raman peaks were fitted with Voigt functions and the inelastic background was modeled by a Shirley background.²¹

Energy calibration was performed by using the Au 4f peak at 84.00 eV for binding energy calibration and the Au M₅N_{6,7}N_{6,7} transition at 2015.8 eV²² for calibration of the kinetic energy

scale. Sample characterization was carried out by hard X-ray photoelectron spectroscopy (HAXPES)²³ measurements using a photon energy of 3000 eV. In addition to this, long-term X-ray exposures were measured of the polymer samples to investigate radiation damage. Core levels were continuously measured with HAXPES for 11 h. No X-ray damage could be ascertained within the time frame of the following spectroscopic measurements (see the [Supporting Information](#)).

The nonradiative decays following resonant core excitation were studied using RAS. A schematic description of the resonant excitation followed by either charge transfer followed by Auger decay (red) or localized Raman decay (yellow) is shown in [Figure 2a](#). Resonant Auger maps were obtained by scanning the photon energy with a 0.5 eV step in the vicinity of the S K-edge while collecting electron energies in the S KL_{2,3}L_{2,3} Auger kinetic energy region (2108–2120 eV).

Near edge X-ray absorption fine structure (NEXAFS) spectroscopy in normal and grazing incidence was carried out to investigate the ordering of polymer chains. The angle between the sample surface normal and incoming photon beam was $\phi = 10^\circ$ for the normal incidence measurements and $\phi = 78^\circ$ for the grazing incidence measurements. Fluorescence yield (FY) NEXAFS is, in comparison to HAXPES and RAS measurements, bulk sensitive on the order of up to μm range. The X-ray emission from polymer samples was recorded using a Bruker XFlash 4010 detector and the excitation energy was scanned over the S K-edge from 2470 to 2495 eV while recording the X-ray emission energy region around sulfur K- β .

RESULTS AND DISCUSSION

HAXPES Measurements. To examine the electronic structure of P(g₄2T-T) and BBL and assess the effects of radiation over time, core level spectroscopic measurements were conducted. [Figure 3](#) presents the HAXPES spectra for the core levels of nitrogen 1s, oxygen 1s, carbon 1s, and sulfur 1s for all polymer blends. Core level spectra were acquired using a photon energy of 3000 eV, and the intensity of each spectrum is normalized relative to the background at the binding energy below the core level peak.

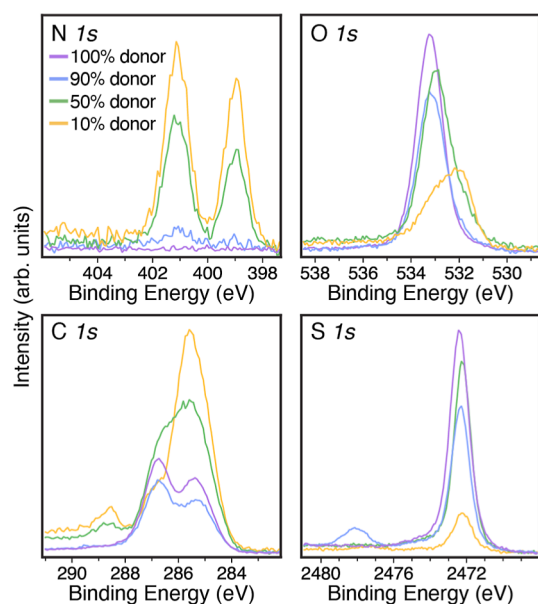


Figure 3. HAXPES spectra of N 1s, O 1s, C 1s, and S 1s of polymer donor–acceptor heterojunctions of different weight blends. An excitation energy of 3000 eV was used for all measurements.

The intensity of the nitrogen 1s core level follows the expected behavior with varied polymer weight blends, considering the stoichiometry of the polymers (Figure 1c). As BBL is diluted with P(g₄2T-T), the nitrogen intensity decreases as this element is only found in the acceptor polymer. The measured binding energy of the nitrogen core level is equivalent between all samples and corresponds well to previously reported XPS measurements of this polymer.²⁴ The oxygen spectra show one dominating feature at a binding energy of 533.2 eV in the sample with 100 and 90% donor, which represents the single bonded oxygen (O–C) found in the donor polymer. A second feature at a lower binding energy (532.0 eV) appears as the amount of BBL increases which relates to the double bonded oxygen (O=C) found in the acceptor polymer.²⁵ In the carbon spectra, the sample with 10% donor displays one dominant feature at 285.5 eV which consists of several components. The low binding energy component of the peak pertains to the carbon–carbon and carbon–hydrogen bonds in the BBL molecule. The component of higher binding energy pertains to carbon–nitrogen bonds and is more prominent in the 10% donor sample compared with the other polymer blends. The second peak at 286.7 eV represents the single bonded carbon and oxygen (C–O) and carbon bonded to sulfur which is present only in the donor P(g₄2T-T). Thus, this peak increases when the relative amount of the donor is increased. The C 1s component at 288.6 eV, found mainly in the 10 and 50% donor samples, originates from the double bonded carbon and oxygen in BBL (C=O).²⁶ The S 1s spectra display the opposite trend in intensity as the nitrogen spectra as sulfur is found only in the donor polymer. One discrepancy from the intensity trend of the main sulfur peak at 2472.4 eV (S–C) is found in the 90% donor sample, which is lower than that of the 50% sample. This is explained by oxidation of the sulfur on the surface, as a second peak is found at higher binding energies (2478.1 eV), demonstrating sulfur bonded to oxygen.²⁵ However, the total sulfur intensity in the 90% sample (sum of both peaks) is larger than that in the 50% sample as expected.

The stability under X-ray exposure was investigated by measuring core levels C 1s, O 1s, and S 1s in the 50% donor sample for 11 h, which showed no considerable level of X-ray-induced damage within the time frame of RAS and NEXAFS measurements. After 11 h of continuous measurement, the intensity decreased for the low binding energy component of C 1s as well as the high binding energy component of O 1s. This implies that a small part of the C–O bonds broke over time. The sulfur peak remains relatively stable in intensity with extended radiation exposure. Resonant Auger measurements were conducted at maximum 9 h where the region of calculated charge-transfer times (2478–2481 eV) was measured within the first 3 h (see the Supporting Information).

X-ray Absorption Measurements. The molecular orientation and ordering of the polymer chains were investigated using NEXAFS spectroscopy which can be used to characterize morphology and ordering in conjugated polymer systems since cross sections depend on the angle between X-ray polarization and orbital orientation.^{11,27,28}

NEXAFS spectra of the P(g₄2T-T) polymer taken at a grazing incidence ($\phi = 78^\circ$) and normal incidence ($\phi = 10^\circ$) are shown in Figure 4c,d. Absorption spectra display the

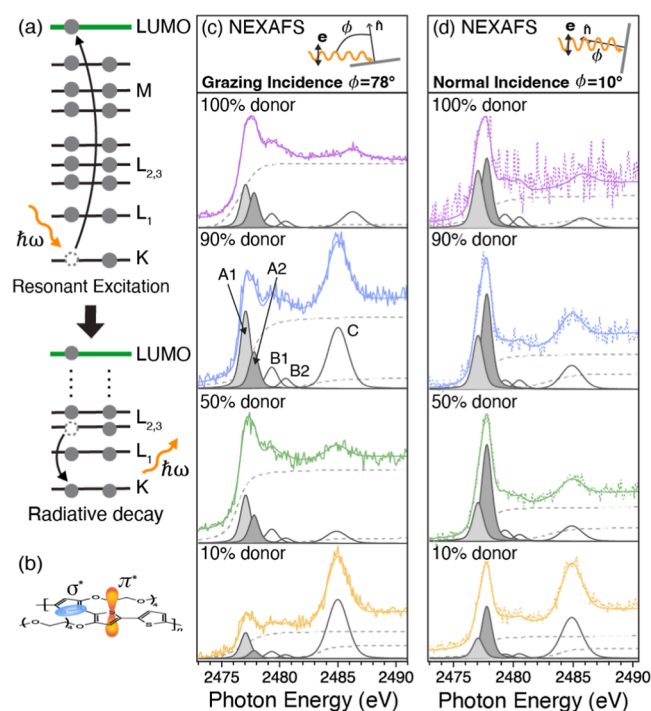


Figure 4. (a) Illustration of the X-ray absorption process and radiative decay in NEXAFS measurements. (b) Schematic depiction of π^* and σ^* orbitals in the donor polymer P(g₄2T-T). NEXAFS spectra of the sulfur K-edge for polymer blends with 10, 50, 90, and 100% donor P(g₄2T-T) at a (c) grazing incidence ($\phi = 78^\circ$) and (d) normal incidence ($\phi = 10^\circ$).

intensity of electronic transitions from the S 1s level to unoccupied molecular orbitals (Figure 4a). Electronic transitions are governed by selection rules, comprised partly of angle of incidence and X-ray polarization.^{7,29} The molecular orbitals of the P(g₄2T-T) polymer are oriented as illustrated in Figure 4b. Intensity variations in the absorption spectra peaks at different angles of incidence indicate the presence of ordering in the polymers.

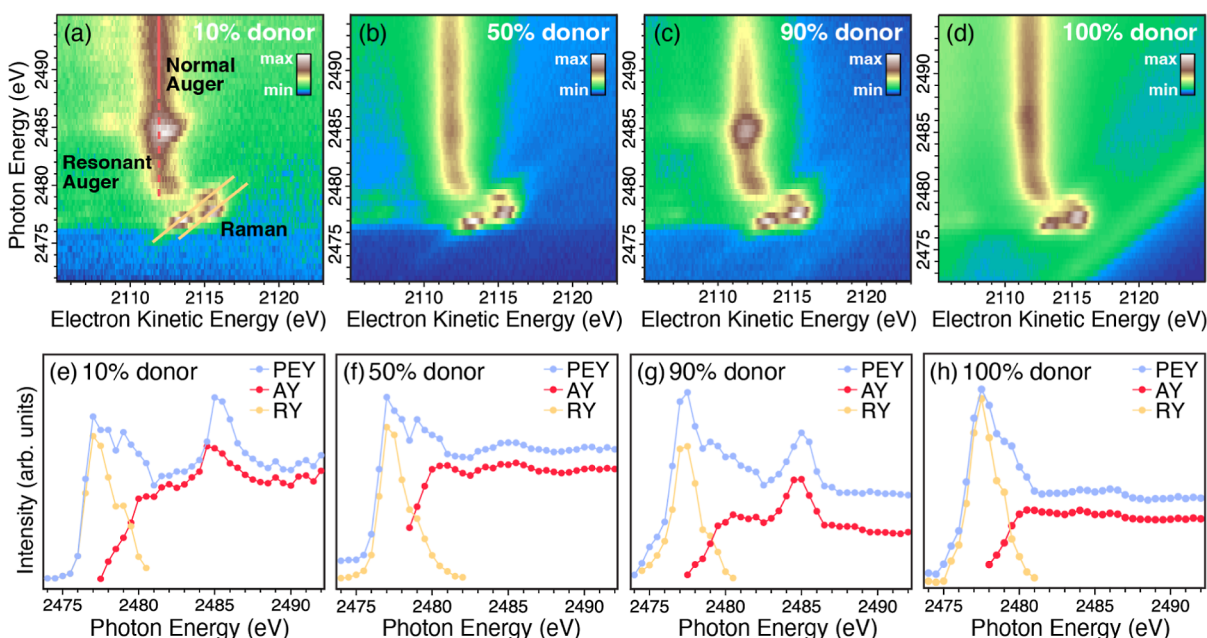


Figure 5. Resonant Auger maps in the sulfur $KL_{2,3}L_{2,3}$ region of polymer blends with (a) 10% donor, (b) 50% donor, (c) 90% donor, and (d) 100% donor. PEY, Auger yield (AY) and Raman yield (RY) obtained from row-wise fit of RAS measurements for polymer blends of (e) 10% donor, (f) 50% donor, (g) 90% donor, and (h) 100% donor.

Intensities were extracted by curve fitting with Voigt functions representing the peaks and arc tangent functions to model the background. The Lorentzian component of the Voigt function was adopted from the sulfur 1s lifetime broadening of 0.52 eV.³⁰ The main peak, labeled A, consists of two peaks lying close to each other at 2477.1 eV (A1) and 2477.8 eV (A2). Peak A1 at a lower energy is assigned to the S 1s $\rightarrow \pi^*$ (S–C) transition and A2 is assigned to the S 1s $\rightarrow \sigma^*$ (S–C) transition.^{29,31–33} These peaks display large differences in intensity for different angles ϕ , suggesting ordering of the sulfur-containing donor polymer. More precisely, they exhibit the opposite trend when the X-ray absorption is measured with normal and grazing incidence, which is expected for π^* and σ^* molecular orbitals. The intensity of the in-plane σ^* orbital (denoted A2) is larger in the normal incidence measurement (Figure 4d) than in the grazing incidence measurement (Figure 4c) which suggests face-on orientation of the thiophene units in P(g₄2T-T). This is consistent with previous studies on the same polymer heterojunction using grazing incidence wide-angle X-ray scattering.⁶

Peak B1 and B2 are found at 2479.5 and 2480.5 eV, respectively. A1, A2, and B1 correspond to coherent states and B2 corresponds to the incoherent charge-transfer state when looking at the resonant Auger maps as shown in Figure 5. The feature at 2485 eV, titled C, corresponds to transitions to a higher energy level in the system attained in both normal and grazing incidence. This feature is more prominent for the 90 and 10% donor samples and is assigned to S 1s $\rightarrow \pi^*$ resonance along a S–O bond found in oxidized sulfur.³⁴ However, sulfur-containing aromatic rings have states in this energy region, see for example, refs 33 and 35. We note that in those cases, there is also charge transfer occurring.

For an ordered film of a planar π -conjugated system containing sulfur, an angular dependence of the X-ray absorption is expected. According to dipole selection rules, when the electric vector is perpendicular to the molecular

plane, core excitations from the sulfur 1s to π^* orbitals are stimulated. Conversely, for σ^* bonds, excitation occurs when the electric vector is parallel to the molecular plane, resulting in opposite behavior within the plane. Ordered polymers probed with polarized X-rays display angular dependence in absorption spectra intensity as expressed by eq 1.⁷

$$I \propto |\langle f | \mathbf{e} \cdot \mathbf{p} | i \rangle|^2 \propto \sin^2 \phi \quad (1)$$

where the angle ϕ between the X-ray polarization axis and the orbital plane influences the transition intensity I from the initial state $|i\rangle$, here 1s, to the molecular orbital final state $|f\rangle$. NEXAFS at intermediate angles of the 50% donor sample were measured, which further corroborates the face-on orientation. This is shown in the Supporting Information. The features associated with π^* and σ^* transitions display a $\sin^2 \phi$ behavior with a 90° offset (see Figure S2b). This behavior is seen for ordered polymers with a face-on orientation.^{36,37} Charge transport is anisotropic and to a greater extent present along the polymer backbone.³⁸ Thus, the orientation and ordering of polymer chains strongly influence the device performance.

The NEXAFS measurements show slight differences in orientation and ordering of the P(g₄2T-T) molecule depending on the weight percentage in relation to BBL. The largest angular dependence of absorption was found in the 50% donor sample. From the NEXAFS spectra, it is also possible to determine that the P(g₄2T-T) polymer is oriented face-on with the sample surface.

Resonant Auger Spectroscopy. With a tunable X-ray source, the sulfur 1s core level in the donor polymer can be resonantly excited and the intensity ratio between subsequent decay channels can be studied (Figure 2). Measuring multiple decay channels following resonant excitation gives insights into electron dynamics during the core-hole lifetime which may be in the subfemtosecond timescale.^{9,39–41} The CHC method was utilized to study ultrafast charge transfer from the sulfur atom in the donor polymer. This method has been successfully

applied to similar systems, providing an estimate of the charge dynamics in van der Waals heterojunctions.⁴²

Decay processes compete at the region of the resonant excitation where the core-excited electron either tunnels away in the material (charge transfer) or stays localized, while an electron at a lower energy level fills the core-hole. The first decay is incoherent and will emit electrons with constant kinetic energies, seen as the vertical features in Figure 5a–d. The constant kinetic energy arises from the Auger-like decay of the core-excited state leaving two holes in the valence since the electron has tunneled away before the core-hole decay—the energy of the electron following the decay depends only on the energy-levels involved and not the photon energy (eq 2).

$$E_{\text{kinetic}}^{\text{Auger}} = E_{\text{binding}}^K - E_{\text{binding}}^{L_{2,3}} - E_{\text{binding}}^{L_{2,3}} + \Delta \quad (2)$$

The kinetic energy of $KL_{2,3}L_{2,3}$ Auger electrons can be found approximately by the binding energies of the involved levels and a correction term Δ accounting for the change of the involved energy levels in the presence of the core-hole.⁴³

The second decay is coherent, and emitted electrons have kinetic energies proportional to the photon energy. The excited electron remains on the site with the core-hole, and the decay of the core-hole involves an electron in another level. The final state is the same as that of a shakeup that can accompany a core level photoionization process. The kinetic energy for electrons emanating from this Raman-like process (eq 3) can be found via energy conservation, i.e., the photoelectric effect.

$$E_{\text{kinetic}}^{\text{Raman}} = \hbar\omega - E_{\text{binding}}^0 - \phi \quad (3)$$

Besides the photon energy \hbar and work function ϕ , the binding energy E_{binding}^0 is the energy difference between initial ground state and core-ionized state energies. We can describe the latter by a sum of states that besides the core-ionized ground state involve one (or several) excited bound electrons which we observe as additional discrete lines in the core level spectrum.⁴⁴ Since the final state is the same for the resonant process (although the path to it is via an intermediate state), the kinetic energy of electrons from the direct ionization with a shakeup satellite and resonant ionization via a core-excited state is the same, giving rise to constant binding energy. This can be seen as the diagonal intensities in the resonant Auger maps seen in Figure 5a–d.

The resonant Auger maps display the intensity of respective decay as a function of excitation energy, where the intensity is represented by the color scale. Above the $K-L_{2,3}L_{2,3}$ resonance (above 2481 eV photon energy), the main feature in the map is the Auger peak at a constant kinetic energy of 2112 eV (indicated by a red vertical line in Figure 5a). This peak is assigned to the transition from the S 1s level to the LUMO in the donor polymer. The sample with 90% donor (Figure 5c) and 10% donor (Figure 5a) shows a distinct increase in intensity related to a transition at a photon energy of 2485 eV. The samples with 50 and 100% donor polymer show no significant increase in intensity at this photon energy.

At a lower excitation energy (2481–2479 eV), the Auger peak shifts to progressively higher kinetic energies. In the same excitation energy region, a new signal appears around a 2116 eV kinetic energy, which disperse linearly when the photon energy is lowered (indicated by yellow diagonal lines in Figure 5a). This signal is termed the coherently excited state or Raman signal, whereas the Auger signal is termed the

incoherent (charge transfer) part. Below 2478 eV, only the coherently excited states remain.

As long as a Raman signal is observed, we are below the core-ionization threshold of the system (here the S 1s ionization potential). In this system, the tunneling away from the site of core-excitation requires an excitation energy of above about 2478 eV as observed for the maps a–d in Figure 5.

The charge-transfer Auger-like state is expected to have constant kinetic energy (reminiscent of normal Auger decay occurring above threshold). However, as discussed above, we observe a shift to higher kinetic energies at lower excitation energies. Here, the tunneled away electron remains bound to the system and aids the polarization screening of the two holes left behind when the core-excited state decays. The amount of kinetic energy shift observed for electrons emanating from this process depends thus on the kinetic energy of the electron that has tunneled away and when during the core-hole lifetime the tunneling occurred. This proximity screening interaction (PSI) enhances the polarization screening by adding a (more or less) diffuse negative charge to the multipole screening of the dicationic final state of the core-hole decay.

This effect is similar to post-collision interaction (PCI) that occurs above the core-ionization threshold, where the interaction between photoelectrons and Auger electrons influence the kinetic energy of the Auger electrons.^{45,46} We stress that the difference from the present case is that here the resonantly excited electron has tunneled away but is still bound to the system. The PSI mechanism is expected to be general for semiconducting and insulating systems where final state charges are polarization screened—indeed in experimental maps of polymers PSI shifts have been present, see for example, ref 11. A limiting case is a metallic interface, where free electrons perfectly screen the final state. This has been observed in resonant Auger maps of Xe on various noble metal surfaces where no PSI shifts occur.¹²

In the Supporting Information, we further discuss PCI and PSI.

By doing a least-squares fit to the intensity profile in the resonant Auger map (see example fit in Figure 2c), the intensity of the coherent Raman channel and the incoherent charge transfer channel can be obtained. Respective partial yield as a function of excitation energy is seen in Figure 5e–h. The partial electron yield (PEY), in the kinetic energy window considered, was obtained by row-wise integration of the intensity in the resonant Auger maps over the photon energy, with the background signal removed. The PEY curves resemble those of the FY NEXAFS spectra recorded with a partial X-ray fluorescence yield with normal incidence (Figure 4d).

CHC Spectroscopy. The electron delocalization time from the LUMO in the donor polymer was measured and compared for different blends of donor–acceptor polymers with varied weight ratios between the donor P(g₂T-T) and acceptor BBL using CHCspectroscopy. This measurement offers a chemical-specific approach (thanks to the resonant X-ray excitation between 1s and unoccupied orbitals) to estimate the intermolecular conductivity originating from the donor polymer in a system where spontaneous electron transfer in the ground state has already occurred. However, the measured systems exhibit a GSET efficiency of only 2%,⁶ indicating that the majority of donor molecules still possess occupied highest occupied molecular orbitals.

The CHC method enables the charge-transfer time of excited electrons on the sulfur atom in the P(g₄2T-T) polymer to be estimated. Using the 1.27 fs core-hole lifetime for the S 1s level as a reference of time³⁰ and the relative intensities of the decays, the charge-transfer time can be calculated using eq 4.

$$\tau_{CT} = \tau_{1s} \frac{I_R}{I_A} \quad (4)$$

The competing localized Raman and delocalized charge-transfer decay processes must occur within the core-hole lifetime, and the probability of charge transfer will influence the intensities in the RAS spectra. Figure 2 describes the resonant and nonresonant excitation of the system to where it relaxes through one of the possible decay channels (radiative decay not included in figure). Above the ionization threshold, the S 1s electron will leave the sulfur atom in an ionized state, followed by a normal Auger decay. Around the resonance, the excited electron will stay localized or tunnel away in the material by charge transfer.

The ratios of the resonant decay intensities are plotted in Figure 6 where the sum of the areas for the respective peak is

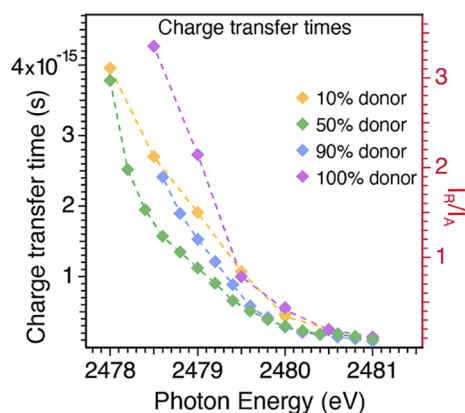


Figure 6. Charge-transfer times calculated from eq 4 for polymer heterojunctions (left axis). Ratio between Raman and Auger features as a function of photon energy (right axis).

compared. From eq 4, the charge-transfer times (τ_{CT}) can be estimated and seen for each polymer blend as shown in Figure 6. The shortest charge-transfer time is recorded for the sample with equal weight percentage of BBL and P(g₄2T-T) and the longest time is obtained for the pure donor polymer P(g₄2T-T). Electrical characterization⁶ of the weight percentage BBL impact on conductivity displays the same behavior as measured charge-transfer times. At a photon energy of 2479 eV, the calculated charge-transfer time is 1.1 fs for the 50% sample. For the samples with 10 and 90% donor, the charge-transfer time for this photon energy is 1.9 and 1.5 fs, respectively. In the pure donor case, the charge-transfer time at a photon energy of 2479 eV is 2.7 fs. This polymer blend displays a slower charge-transfer time at almost all photon energies.

Two separate behaviors can be observed in Figure 6: a low excess energy regime where the electron dynamics are blend-dependent and a region above 2479.5 eV where the different systems are similar. Recalling that the objective with this particular polymer blend is to optimize ground-state electron transfer by mixing polymers in a bulk heterojunction (Figure 1), we can imagine that a BBL-poor or BBL-rich blend will

increase or decrease the volumes with only P(g₄2T-T) in them as the polymers are not totally miscible. A core excited state in the sulfur-containing polymer can decay locally on the same polymer (intrapolymer) or via charge transfer to a neighbor polymer (interpolymer), which may be BBL or another P(g₄2T-T). By changing the blend ratio, we can observe the effect of the two kinds of interpolymer decays on the charge-transfer dynamics.

At low excitation energies, the presence of acceptor chains is important as the additional decay channels allow electron transfer from the site with the core-hole to occur efficiently. The 50% blend has the most efficient interpolymer transfer, whereas 10% or 90% acceptor are less efficient. It is clear that the 0% acceptor is the least efficient, which is not surprising since the acceptor density of states is not present to offer additional pathways for the decay of the core-excited state. If the acceptor density of states determines the tunneling efficiency, the 10% donor blend would exhibit the fastest charge transfer. Since acceptor density of states does not capture the behavior, we need to consider the interface and orbital overlaps between the different molecules.

The rate of decay of the core-excited state can be described by Fermi's golden rule

$$\Gamma = \frac{2\pi}{\hbar} \sum_f |\langle f | \mathbf{Q} | i \rangle|^2 \rho(E) \quad (5)$$

which describes the transition rate between final state f and initial state i coupled by the operator \mathbf{Q} weighted by the density of states. The decay from the core-excited N -electron system into a $N - 1$ system with an electron in the continuum may be described by the matrix element

$$\langle \phi_1 \phi_2 | e^2 / r | \phi_c \phi_e \rangle \langle \Psi_i^{N-2} | \Psi_f^{N-2} \rangle \quad (6)$$

with the approximation that the $N - 2$ electrons not involved only screen the electrons in orbitals 1 and 2 in the final state and the core-hole and excited electron in the initial state.⁴⁷ This decay process is governed by the Coulomb operator, i.e., $\mathbf{Q} = e^2/r$. Together with eq 6, this matrix element describes a decay process that depends on the overlap between the electron density near the core-hole ϕ_c . The rate described is thus a localized probe of orbital overlaps and the density of states. In the case of 0%, an overlap is necessary between molecules that are the same. Adding acceptor to the blend introduces heteromolecular overlaps into the sum. This explains the difference in the transition rate between the polymer blends and the pure donor case.

The rate of charge transfer depends on both the orbital overlap and density of states. For the 50% blend, we find an optimum in the sense that this rate is the fastest. This suggests that charge transfer from the donor to the acceptor, meaning interpolymer charge transfer, is the most efficient pathway. This is also the system with the largest degree of ordering as seen in the NEXAFS spectra. A larger overlap in this more-ordered 50% blend may be explained by a larger matrix element than in the less-ordered case. Changing the blend also changes the interface area between the polymers, which affects the density of states. In this case, we find this optimum at 50% while for other polymers this optimum will be dependent on the relative size of the molecules. For PCPDTBT:PCBM, Johansson finds the optimum at a 1:2 weight ratio.¹¹ In our case, we see the effects of not only overlap but also how ordering of the polymers affects charge transfer between them.

CONCLUSIONS

The NEXAFS spectra of P(g₄2T-T) blended with BBL have been recorded using different incident angles of the incoming light and showed the ordering of the thiophene chains in the donor polymer. Suppression of the π^* signal relative to the σ^* in grazing incidence suggest that the thiophenes in P(g₄2T-T) are oriented face-on to the surface. The largest degree of ordering was found in the sample with an equal amount of donor and acceptor polymer. Maps of the resonant Auger spectra taken in the vicinity of the S K-edge were used to employ the CHC approach to determine charge-transfer times for different blends of the two polymers. We observe ultrafast charge dynamics from the unoccupied level in the sulfur atom of the p-type polymer. Electron delocalization times were derived which occurred in the as/fs regime for all polymer blends, with the fastest charge-transfer time measured in the sample with equal amount of donor (P(g₄2T-T) and acceptor (BBL) polymer. CHC spectroscopy has previously been used to gain information on the charge dynamics of polymeric systems for organic solar cells, where the shortest charge-transfer time occurred for the device blend yielding the best performance in the solar cell application.¹¹ Sloboda and co-workers found that the fastest charge transfer for PbS quantum dots occur for the size of quantum dot that yield best photovoltaic performance.¹³ Here, we find that the local charge-transfer optimum occurs for the polymer blend that gives optimal macroscopic performance when conductivity is considered. While the conductivity of this blend increased due to doping by GSET, we also show here that the charge transfer from the LUMO of the donor is the fastest for this blend. We suggest that this measure of local conductivity can be used to predict macroscopic performance measures that are dependent on charge mobility. Since CHC spectroscopy is a chemically specific method, it could also be used as a tool to analyze candidate donor/acceptor systems where chemical changes are expected to alter device properties and to gain insights into the atomic origin of both favorable and unfavorable functionality.

ASSOCIATED CONTENT

Supporting Information

The Supporting Information is available free of charge at <https://pubs.acs.org/doi/10.1021/acs.jpcc.3c05665>.

Additional HAXPES spectra of radiation impact, NEXAFS spectra at intermediate angles, examples of resonant Auger spectral fitting, and schematic comparison of PCI and PSI (PDF)

AUTHOR INFORMATION

Corresponding Author

Elin Berggren – Division of X-ray Photon Science, Department of Physics and Astronomy, Uppsala University, SE-751 20 Uppsala, Sweden; orcid.org/0000-0001-8693-0492; Email: elin.berggren@physics.uu.se

Authors

Yi-Chen Weng – Division of X-ray Photon Science, Department of Physics and Astronomy, Uppsala University, SE-751 20 Uppsala, Sweden; orcid.org/0000-0002-8676-8605

Qifan Li – Laboratory of Organic Electronics, Department of Science and Technology, Linköping University, SE-60174 Norrköping, Sweden

Chi-Yuan Yang – Laboratory of Organic Electronics, Department of Science and Technology, Linköping University, SE-60174 Norrköping, Sweden; orcid.org/0000-0003-4270-1131

Fredrik O. L. Johansson – Division of Applied Physical Chemistry, Department of Chemistry, KTH-Royal Institute of Technology, SE-100 44 Stockholm, Sweden; Sorbonne Université, CNRS, Institut des NanoSciences de Paris-INSP, F 75005 Paris, France; orcid.org/0000-0002-6471-1093

Ute B. Cappel – Division of Applied Physical Chemistry, Department of Chemistry, KTH-Royal Institute of Technology, SE-100 44 Stockholm, Sweden; orcid.org/0000-0002-9432-3112

Magnus Berggren – Laboratory of Organic Electronics, Department of Science and Technology, Linköping University, SE-60174 Norrköping, Sweden; orcid.org/0000-0001-5154-0291

Simone Fabiano – Laboratory of Organic Electronics, Department of Science and Technology, Linköping University, SE-60174 Norrköping, Sweden; orcid.org/0000-0001-7016-6514

Andreas Lindblad – Division of X-ray Photon Science, Department of Physics and Astronomy, Uppsala University, SE-751 20 Uppsala, Sweden; orcid.org/0000-0002-9188-9604

Complete contact information is available at: <https://pubs.acs.org/doi/10.1021/acs.jpcc.3c05665>

Notes

The authors declare no competing financial interest.

ACKNOWLEDGMENTS

The authors thank the experimental team at the KMC-1 beamline and HZB for allocation of beamtime with proposal no.221-10967-ST. We extend our gratitude to Renee Kroon from Linköping University for providing the polymer P(g₄2T-T) used in this study. A.L. and E.B. acknowledge the financial support from the Swedish Research Council grant no. 2018-05336. F.O.L.J. acknowledges support from the Swedish Research Council (grant 2020-06409).

REFERENCES

- (1) Fahlman, M.; Fabiano, S.; Gueskine, V.; Simon, D.; Berggren, M.; Crispin, X. Interfaces in organic electronics. *Nat. Rev. Mater.* **2019**, *4*, 627–650.
- (2) Berggren, M.; Glowacki, E. D.; Simon, D. T.; Stavrinidou, E.; Tybrandt, K. In vivo organic bioelectronics for neuromodulation. *Chem. Rev.* **2022**, *122*, 4826–4846.
- (3) Guo, X.; Baumgarten, M.; Müllen, K. Designing π -conjugated polymers for organic electronics. *Prog. Polym. Sci.* **2013**, *38*, 1832–1908.
- (4) Lei, T.; Cao, Y.; Fan, Y.; Liu, C.-J.; Yuan, S.-C.; Pei, J. High-performance air-stable organic field-effect transistors: isoindigo-based conjugated polymers. *J. Am. Chem. Soc.* **2011**, *133*, 6099–6101.
- (5) Boudreault, P.-L. T.; Najari, A.; Leclerc, M. Processable low-bandgap polymers for photovoltaic applications. *Chem. Mater.* **2011**, *23*, 456–469.
- (6) Xu, K.; Sun, H.; Ruoko, T.-P.; Wang, G.; Kroon, R.; Kolhe, N. B.; Puttison, Y.; Liu, X.; Fazzi, D.; Shibata, K.; et al. Ground-state electron transfer in all-polymer donor–acceptor heterojunctions. *Nat. Mater.* **2020**, *19*, 738–744.
- (7) Stöhr, J. *NEXAFS Spectroscopy*; Springer Science & Business Media, 2013; Vol. 25.

- (8) Armen, G. B.; Aksela, H.; Åberg, T.; Aksela, S. The resonant Auger effect. *J. Phys. B: At., Mol. Opt. Phys.* **2000**, *33*, R49–R92.
- (9) Brühwiler, P. A.; Karis, O.; Mårtensson, N. Charge-transfer dynamics studied using resonant core spectroscopies. *Rev. Mod. Phys.* **2002**, *74*, 703–740.
- (10) Johansson, F. O.; Cappel, U. B.; Fondell, M.; Han, Y.; Gorgoi, M.; Leifer, K.; Lindblad, A. Tailoring ultra-fast charge transfer in MoS₂. *Phys. Chem. Chem. Phys.* **2020**, *22*, 10335–10342.
- (11) Johansson, F.; Ivanović, M.; Svanström, S.; Cappel, U. B.; Peisert, H.; Chassé, T.; Lindblad, A. Femtosecond and attosecond electron-transfer dynamics in PCPDTBT:PCBM bulk heterojunctions. *J. Phys. Chem. C* **2018**, *122*, 12605–12614.
- (12) Johansson, F. O.; Berggren, E.; Cornetta, L. M.; Céolin, D.; Fondell, M.; Ågren, H.; Lindblad, A. Resonant Auger spectroscopy on solid xenon on gold, silver, and copper substrates. *Phys. Rev. A* **2023**, *107*, 032802.
- (13) Sloboda, T.; Johansson, F. O.; Kammlander, B.; Berggren, E.; Svanström, S.; Fernández, A. G.; Lindblad, A.; Cappel, U. B. Unravelling the ultrafast charge dynamics in PbS quantum dots through resonant Auger mapping of the sulfur K-edge. *RSC Adv.* **2022**, *12*, 31671–31679.
- (14) Johansson, F. O.; Chen, X.; Eriksson, O.; Sanyal, B.; Lindblad, A. Interlayer charge transfer in tin disulphide: Orbital anisotropy and temporal aspects. *Phys. Rev. B* **2020**, *102*, 035165.
- (15) Oropeza, F. E.; Barawi, M.; Alfonso-González, E.; de la Peña O'Shea, V. A.; Trigo, J. F.; Guillén, C.; Saiz, F.; Villar-García, I. J. Understanding ultrafast charge transfer processes in SnS and SnS₂: using the core hole clock method to measure attosecond orbital-dependent electron delocalisation in semiconducting layered materials. *J. Mater. Chem. C* **2021**, *9*, 11859–11872.
- (16) Chen, Z.; Xiong, H.; Zhang, H.; Gao, C.; Cheng, Y.; Papalazarou, E.; Perfetti, L.; Marsi, M.; Rueff, J.-P. Ultrafast electron energy-dependent delocalization dynamics in germanium selenide. *Commun. Phys.* **2021**, *4*, 138.
- (17) Wu, H.-Y.; Yang, C.-Y.; Li, Q.; Kolhe, N. B.; Strakosas, X.; Stoeckel, M.-A.; Wu, Z.; Jin, W.; Savvakis, M.; Kroon, R.; et al. Influence of molecular weight on the organic electrochemical transistor performance of ladder-type conjugated polymers. *Adv. Mater.* **2022**, *34*, 2106235.
- (18) Gorgoi, M.; Svensson, S.; Schäfers, F.; Öhrwall, G.; Mertin, M.; Bressler, P.; Karis, O.; Siegbahn, H.; Sandell, A.; Rensmo, H.; et al. The high kinetic energy photoelectron spectroscopy facility at BESSY progress and first results. *Nucl. Instrum. Methods Phys. Res., Sect. A* **2009**, *601*, 48–53.
- (19) Patanen, M.; Aksela, S.; Urpeläinen, S.; Kantia, T.; Heinäsmäki, S.; Aksela, H. Free atom 4f photoelectron spectra of Au, Pb, and Bi. *J. Electron Spectrosc. Relat. Phenom.* **2011**, *183*, 59–63.
- (20) Kukk, E. *Spectrum Analysis by Curve Fitting (SPANCF)-Macro Package for Igor Pro*, 2012.
- (21) Shirley, D. A. High-resolution X-ray photoemission spectrum of the valence bands of gold. *Phys. Rev. B: Solid State* **1972**, *5*, 4709–4714.
- (22) Seah, M. AES energy calibration of electron spectrometers. IV. A re-evaluation of the reference energies. *J. Electron. Spectrosc. Relat. Phenom.* **1998**, *97*, 235–241.
- (23) Kalha, C.; Fernando, N. K.; Bhatt, P.; Johansson, F. O.; Lindblad, A.; Rensmo, H.; Medina, L. Z.; Lindblad, R.; Siol, S.; Jeurgens, L. P.; et al. Hard x-ray photoelectron spectroscopy: a snapshot of the state-of-the-art in 2020. *J. Phys.: Condens. Matter* **2021**, *33*, 233001.
- (24) Yang, C.-Y.; Stoeckel, M.-A.; Ruoko, T.-P.; Wu, H.-Y.; Liu, X.; Kolhe, N. B.; Wu, Z.; Puttison, Y.; Musumeci, C.; Massetti, M.; et al. A high-conductivity n-type polymeric ink for printed electronics. *Nat. Commun.* **2021**, *12*, 2354.
- (25) Chastain, J.; King, R. C. *Handbook of X-ray Photoelectron Spectroscopy*; Perkin-Elmer Corporation, 1992; Vol. 40, p 221.
- (26) Chen, Y.; Wu, H.-Y.; Yang, C.-Y.; Kolhe, N. B.; Jenekhe, S. A.; Liu, X.; Braun, S.; Fabiano, S.; Fahlman, M. In Situ Spectroscopic and Electrical Investigations of Ladder-type Conjugated Polymers Doped with Alkali Metals. *Macromolecules* **2022**, *55*, 7294–7302.
- (27) Borges, B.; Veiga, A. G.; Tzounis, L.; Laskarakis, A.; Logothetidis, S.; Rocco, M. Molecular orientation and ultrafast charge transfer dynamics studies on the P3HT: PCBM blend. *J. Phys. Chem. C* **2016**, *120*, 25078–25082.
- (28) Tong, M.; Cho, S.; Rogers, J. T.; Schmidt, K.; Hsu, B. B.; Moses, D.; Coffin, R. C.; Kramer, E. J.; Bazan, G. C.; Heeger, A. J. Higher molecular weight leads to improved photoresponsivity, charge transport and interfacial ordering in a narrow bandgap semiconducting polymer. *Adv. Funct. Mater.* **2010**, *20*, 3959–3965.
- (29) Aygül, U.; Batchelor, D.; Dettinger, U.; Yilmaz, S.; Allard, S.; Scherf, U.; Peisert, H.; Chassé, T. Molecular orientation in polymer films for organic solar cells studied by NEXAFS. *J. Phys. Chem. C* **2012**, *116*, 4870–4874.
- (30) Campbell, J.; Papp, T. Widths of the atomic K–N7 levels. *Atomic Data Nucl. Data Tables* **2001**, *77*, 1–56.
- (31) Martins, J. B.; de Moura, C. E.; Goldsztejn, G.; Travnikova, O.; Guillemin, R.; Ismail, I.; Journal, L.; Koulentianos, D.; Barbatti, M.; Lago, A. F.; et al. Electron delocalisation in conjugated sulfur heterocycles probed by resonant Auger spectroscopy. *Phys. Chem. Chem. Phys.* **2022**, *24*, 8477–8487.
- (32) Hitchcock, A.; Horsley, J.; Stöhr, J. Inner shell excitation of thiophene and thiolane: Gas, solid, and monolayer states. *J. Chem. Phys.* **1986**, *85*, 4835–4848.
- (33) George, G. N.; Hackett, M. J.; Sansone, M.; Gorbaty, M. L.; Kelemen, S. R.; Prince, R. C.; Harris, H. H.; Pickering, I. J. Long-range chemical sensitivity in the sulfur K-edge X-ray absorption spectra of substituted thiophenes. *J. Phys. Chem. A* **2014**, *118*, 7796–7802.
- (34) Winter, I.; Reese, C.; Holmes, J.; Heywang, G.; Jonas, F. The thermal ageing of poly (3, 4-ethylenedioxythiophene). An investigation by X-ray absorption and X-ray photoelectron spectroscopy. *Chem. Phys.* **1995**, *194*, 207–213.
- (35) Mijovilovich, A.; Pettersson, L. G.; de Groot, F. M.; Weckhuysen, B. M. Functional Groups and Sulfur K-Edge XANES Spectra: Divalent Sulfur and Disulfides. *J. Phys. Chem. A* **2010**, *114*, 9523–9528.
- (36) Yannoulis, P.; Dudde, R.; Frank, K.; Koch, E. Orientation of aromatic hydrocarbons on metal surfaces as determined by NEXAFS. *Surf. Sci.* **1987**, *189–190*, 519–528.
- (37) Stöhr, J.; Outka, D. Determination of molecular orientations on surfaces from the angular dependence of near-edge x-ray-absorption fine-structure spectra. *Phys. Rev. B: Condens. Matter Mater. Phys.* **1987**, *36*, 7891–7905.
- (38) Nahid, M. M.; Gann, E.; Thomsen, L.; McNeill, C. R. NEXAFS spectroscopy of conjugated polymers. *Eur. Polym. J.* **2016**, *81*, 532–554.
- (39) Föhlisch, A.; Feulner, P.; Hennies, F.; Fink, A.; Menzel, D.; Sanchez-Portal, D.; Echenique, P. M.; Wurth, W. Direct observation of electron dynamics in the attosecond domain. *Nature* **2005**, *436*, 373–376.
- (40) Johansson, F. O.; Sassa, Y.; Edvinsson, T.; Lindblad, A. Gone in 23 Attoseconds: Charge transfer in resonantly core excited black phosphorous. *arXiv* **2020**, arXiv:2003.13394 Preprint.
- (41) Garcia-Basabe, Y.; Ceolin, D.; Zarbin, A. J.; Roman, L. S.; Rocco, M. L. M. Ultrafast interface charge transfer dynamics on P3HT/MWCNT nanocomposites probed by resonant Auger spectroscopy. *RSC Adv.* **2018**, *8*, 26416–26422.
- (42) Garcia-Basabe, Y.; Steinberg, D.; Daminelli, L. M.; Mendoza, C. D.; de Souza, E. A. T.; Vicentin, F. C.; G Larrudé, D. Charge-transfer dynamics in van der Waals heterojunctions formed by thiophene-based semiconductor polymers and exfoliated frackeite investigated from resonantly core-excited electrons. *Phys. Chem. Chem. Phys.* **2021**, *23*, 16795–16805.
- (43) Åberg, T. Unified theory of Auger electron emission. *Phys. Scr.* **1992**, *1992*, 71–76.
- (44) Martin, R.; Shirley, D. Theory of core-level photoemission correlation state spectra. *J. Chem. Phys.* **1976**, *64*, 3685–3689.

(45) Straten, P.; Morgenstern, R.; Niehaus, A. Angular dependent post-collision interaction in Auger processes. *Z. Phys. D: At., Mol. Clusters* **1988**, *8*, 35–45.

(46) Velasquez, N.; Travnikova, O.; Guillemin, R.; Ismail, I.; Journal, L.; Martins, J. B.; Koulentianos, D.; Céolin, D.; Fillaud, L.; Rocco, M. L. M.; et al. Generalization of the post-collision interaction effect from gas-phase to solid-state systems demonstrated in thiophene and its polymers. *Phys. Rev. Res.* **2023**, *5*, 013048.

(47) Eberhardt, W.; Bradshaw, A.; Freund, H.; Hoffmann, F.; Kühlenbeck, H.; Martensson, N.; Menzel, D.; Nilsson, A.; Williams, G.; Woodruff, D. *Applications of Synchrotron Radiation: High-resolution Studies of Molecules and Molecular Adsorbates on Surfaces*; Springer, 1995; Chapter 6.